Measuring the current-phase relation of a Josephson junction

Doorn, Julian van

Measuring the current-phase relation of a Josephson junction

Thesis

submitted in partial fulfillment of the
requirements for the degree of

Bachelor of Science
in
Physics

Author :	J.C.B. van Doorn
Student ID :	s2518074
Supervisor :	M. Rog, MSc
	Dr. K. Lahabi
Second corrector :	Prof. Dr. J. Aarts

Leiden, The Netherlands, June 30, 2023

Measuring the current-phase relation of a Josephson junction

J.C.B. van Doorn

Huygens-Kamerlingh Onnes Laboratory, Leiden University
P.O. Box 9500, 2300 RA Leiden, The Netherlands

June 30, 2023

Abstract

The current through a Josephson junction is governed by the current-phase relation (CPR) that depends on the phase difference between the electrodes. Notable applications are qubits, Josephson diodes and microscopic imaging techniques. This thesis presents a method to measure the CPR based on [1]. The junction under study is incorporated into a superconducting loop that is inductively coupled to a dc-SQUID magnetometer. The measured flux is proportional to the junction's phase and by controlling the current through the junction's loop it is possible to directly measure the CPR. This thesis outlines several important considerations and constraints of this method. Furthermore we provide CPR measurements of a superconductor-normal-superconductor (SNS) junction made from Nb and Cu. It shows a clear temperature dependence with a qualitative change in shape as well as a quantitative change in amplitude of the current-phase relation. These results are in agreement with theory. In the future a flux-locked loop can be used to further improve the measurements.

Contents

Conventions

In this thesis we take $e = |e|$ meaning the electron has a charge of $-e$. The charge of a Cooper pair (denoted e^* in *Introduction to Superconductivity* by Tinkham) is then $-2e$. The mass of a Cooper pair (denoted m^* in *Introduction to Superconductivity* by Tinkham) is two times the mass of a single electron, denoted by $2m_e$ in this thesis.

Chapter 1

Introduction

Josephson junctions have a wide variety of applications such as qubits[3, 4]; superconducting electronics through Josephson diodes[5, 6]; and microscopic imaging techniques[7–9]. The behaviour of a Josephson junction is governed by its current-phase relation (CPR). Probing the CPR can lead to new insights and applications. Par example by measuring the CPR it is possible to if the junction's behaviour is ballistic or diffusive[10–12] and it has shown the existence of 0-π and φ_0 junctions[1, 10, 13, 14] as well as non-2π periodic CPRs[11].

In our group there is an additional interest in the CPR of homogenous Sr_2RuO_4 rings. Recent work by Lahabi *et al.* provides evidence for the existence of chiral domain walls in these rings that act as Josephson junctions.[15] As such, homogenous Sr_2RuO_4 rings show dc-SQUID like behaviour without the presence of constrictions, grain boundaries or an interface with a different material. Definitive proof for chiral domain walls can be found by measuring the Josephson energy.[15, 16] The most elegant way to determine the Josephson energy is by measuring the CPR.

Furthermore, our group has been characterising the behaviour of Josephson junctions containing $La_{0.7}Sr_{0.3}MnO_3$ (LSMO). LSMO is a half-metallic ferromagnet and spin triplet supercurrents were observed. Transport measurements have been performed and the magnetic field dependence of the critical current was determined. However, there are still several open questions regarding the observed behaviours and their origins.[17] New insights might be acquired by measuring the current-phase relation.

Two of the key benefits of our method is that it directly measures the full

CPR and only needs a simple analysis. Details on the analysis can be found in Section 3.1. An alternative method uses a strongly asymmetric dc-SQUID where the junction with a much smaller critical current dominates the behaviour of the dc-SQUID.[10, 18] A downside of this method is that it is much more difficult to produce the samples. Microwave measurements have been used to determine the skewness of the CPR but cannot probe the CPR directly.[19]

The next chapter will lay a theoretical foundation for our method. Chapter 3 delves deeper into our method, presents numerical calculations to guide our expectations. Then our results are presented on a per sample. Finally a conclusion is drawn and we sketch an outlook for future research.

Chapter 2

Theory

2.1 Superconductors

The most well known properties of superconductors are their perfect conductivity[1] and diamagnetism[2]. A microscopic description of the effect is given by Bardeen, Cooper and Schieffer (BCS theory) and phenomenologically by the Ginzburg-Landau theory.[2] This section will highlight the relevant parts of these theories for our research.

BCS theory shows that superconductivity, on the atomic scale, is a result of the creation of paired electrons called Cooper pairs. Cooper pairs form from an phonon-mediated attractive interaction that overcomes the Coulomb repulsion between two electrons.[20] Electrons have half-integer spin. This means a Cooper pair, consisting of two electrons, has integer spin. As such Cooper pairs are bosons.

Bosons, contrary to fermions, can occupy the same quantum state. Below their critical temperature bosons form a condensate. All Cooper pairs in the condensate occupy the same macroscopic wavefunction[3].

$$\Psi = |\Psi| \exp(i\varphi) \tag{2.1}$$

Both $|\Psi|$ and φ are functions of position. The behaviour of this wave function is described by the Ginzburg-Landau theory. In this theory, $|\Psi|^2$ is a measure

[1] Discovered by H.K. Onnes in 1911.
[2] Discovered by W. Meissner and R. Ochsenfeld in 1933.
[3] This is by definition of a 'condensate' the case.

for the density of Cooper pairs (units of m^{-3}). The super current density($\mathrm{A} \cdot \mathrm{m}^{-2}$) in a superconductor is governed by ϕ (and $\vec{A}$)[4]:

$$\vec{J_s} = e^*|\Psi|^2\vec{v_s} = \frac{e^*}{m^*}|\Psi|^2\left(\hbar\nabla\varphi - \frac{e^*}{c}\vec{A}\right) \overset{\text{SI}}{=} \frac{e}{m_e}|\Psi|^2\left(\hbar\nabla\varphi + 2e\vec{A}\right) \tag{2.2}$$

2.1.1 Characteristic length scales

There are two important length scales for superconductors. We will focus on these length scales mainly in relation to the Ginzburg-Landau theory. Figure 2.1 schematically depicts the two length scales.

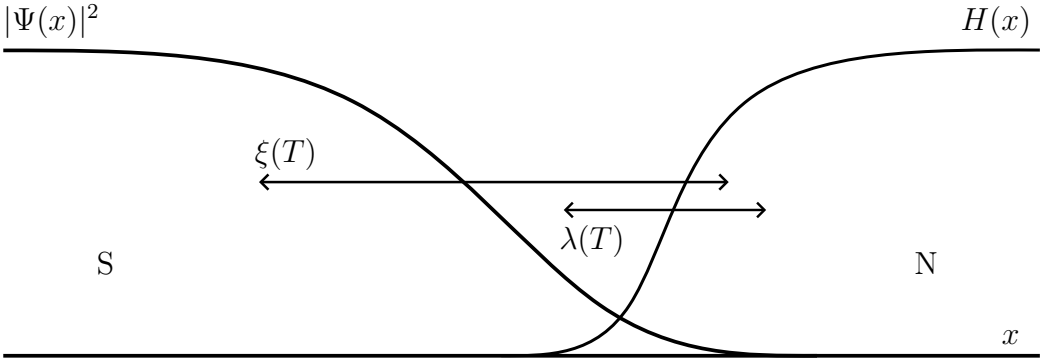

Figure 2.1: *Schematic depiction of the characteristic lengths ξ and λ. The Cooper-pair density $|\Psi(x)|^2$, also referred to as n_s, falls off on a scale ξ. The magnetic field gets shielded by the superconductor using a shielding current and falls off on a scale λ. The S and N denote the 'superconducting' and 'normal' regimes respectively.*

The first is the scale over which the Cooper-pair density can change. This is the so called coherence length, $\xi = \xi(T)$. ξ decreases when the temperature increases.[2]

The second length scale is the penetration depth $\lambda = \lambda(T)$. It is a measure for the 'stiffness' of the phase. A small λ means φ can change easily. This means larger super currents are possible. The currents can screen magnetic fields which penetrate roughly on the same length scale. The penetration depth in Ginzburg-Landau theory at 0 K is given by[5]:

$$\lambda(0) = \sqrt{\frac{m^*c^2}{4\pi|\Psi|^2e^{*2}}} \overset{\text{SI}}{=} \sqrt{\frac{m_e}{2|\Psi|^2e^2\mu_0}} \tag{2.3}$$

[4]See *Introduction to Superconductivity* equation 4.14a.
[5]See *Introduction to Superconductivity* equation 4.8.

The penetration depth too is dependent on temperature and decreases for higher temperatures. For more information on length scales the reader is referred to *Introduction to Superconductivity* by Tinkham.

2.2 Josephson effect

When two superconductors are separated by a weak link[6] a supercurrent can flow between them. Josephson showed in 1962 that for two superconductors separated by an insulating tunnelling barrier the current is given by[2]:

$$I_s = I_c \sin(\Delta\varphi) \tag{2.4}$$

Where $\Delta\varphi = \varphi_2 - \varphi_1$ is the difference in phase between the two condensates as described by Ginzburg-Landau theory (Equation 2.1). Furthermore I_c is the critical current of the junction. This equation is generally known as the first Josephson equation. The relation between I_s and $\Delta\varphi$ is the CPR. In general this does not have to be purely sinusoidal.[21]

In the more general case the gauge invariant phase[7] is used:

$$\gamma = \Delta\varphi - \frac{2\pi}{\Phi_0} \int \vec{A} \cdot d\vec{l} \tag{2.5}$$

We are required to do so as $\Delta\varphi$ is not uniquely determined for a given physical situation whilst I_s is.[2] It transforms $I_c \sin(\Delta\varphi) \rightarrow I_c \sin(\gamma)$. Furthermore we can extend to the case where the CPR is not purely sinusoidal by replacing $\sin(\gamma) \rightarrow f(\gamma)$:

$$I_s = I_c f(\gamma) \tag{2.6}$$

$f(\gamma)$ is called the current-phase relation and I_s has a maximum amplitude of I_c. In general f has the following properties[21]:

$$f(\gamma) = f(\gamma + 2\pi) \quad f(\gamma) = -f(-\gamma) \quad f(2\pi n) = f(\pi m) = 0 \tag{2.7}$$

With $m, n \in \mathcal{N}$. The last statement is not always true. There have been reports of 4π periodic CPRs.[11]

[6] This can be an insulator, normal metal, different superconductor or a constriction.

[7] See *Introduction to Superconductivity* equation 6.11. The equation is valid in both Gaussian and SI units.

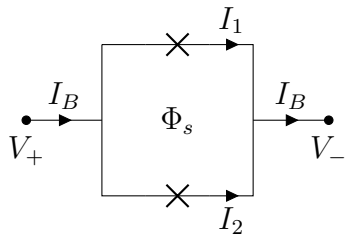

Figure 2.2: *Schematic depiction of a dc-SQUID. The loop contains two Josephson junctions (denoted with the crosses). The total current $I_B = I_1 + I_2$ and a voltage $V_s = V_+ - V_-$ can be measured between the two contacts.*

2.3 dc-SQUID magnetometers

It is clear from Equation 2.4 that CPRs do not describe the behaviour for currents larger than I_c. Instead, above I_c junctions operate in the 'dynamic regime' governed by the second Josephson relation[2]:

$$V_s = \frac{\Phi_0}{2\pi}\frac{\partial(\Delta\varphi)}{\partial t} \tag{2.8}$$

When two junctions are used parallel to each other in a loop (Figure 2.2) then the dynamic regime starts at $2I_c$. This is assuming the junctions are symmetric. The current in a superconductor is dependent on $\vec{A}$ (Equation 2.2). That means that we can tune the phase by applying a magnetic field. The maximum current we can pass through the parallel junctions is given by[2, 7]:

$$I_{\max} = 2I_c \left|\cos\left(\pi\frac{\Phi_s}{\Phi_0}\right)\right| \tag{2.9}$$

With Φ_s the magnetic flux enclosed by the loop. This behaviour gives rise to the 'dc-SQUID interference pattern' (SQI). Such a pattern is shown in Figure 2.3. Most importantly, this pattern is exactly Φ_0 periodic independent of any device geometries. As such it is very easy to calibrate. Two parameters are important for the sensitivity and hysteresis[7]:

$$\beta_c = \frac{2\pi}{\Phi_0} I_c R^2 C \qquad \text{(Stewart-McCumber parameter)}$$

$$\beta_L = \frac{2LI_0}{\Phi_0} \qquad \text{(screening parameter)}$$

Ideally β_c is minimized and $\beta_L \approx 1$.[8]

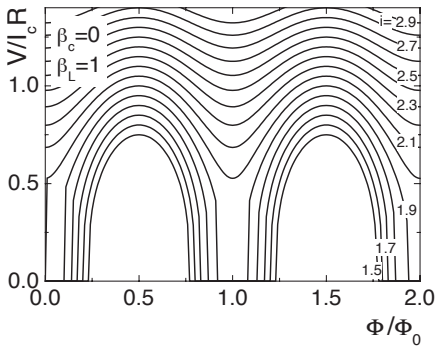

Figure 2.3: *Normalized dc-SQUID voltage (V/I_cR) over normalized flux (Φ_a/Φ_0). The lines are for constant current $i = I_b/2I_c$. The two parameters are $\beta_c = 0$ and 1. The figure has been adapted from [7].*

2.3.1 dc-SQUID magnetometer readout

By passing a bias current $I_B > 2I_c$ through the dc-SQUID a voltage V_s develops. By measuring this voltage and applying an external field you can determine the calibration curve of the dc-SQUID magnetometer. Since the periodicity of the SQI is always Φ_0 this allows you to determine the relation between V_s and Φ. Figure 2.3 shows that there are (small) regions where the dc-SQUID's response is linear. In this region we define the transfer function[8]:

$$H = \left.\frac{\partial V_s}{\partial \Phi}\right|_{I_B} \tag{2.10}$$

In the example figure the most sensitive response is obtained for $I_B = 2i$. After the calibration you can determine the flux through the dc-SQUID by measuring its voltage.

For more information on dc-SQUID magnetometry the reader is referred to [2, 7, 22].

Chapter 3

Method

Our method is based on Frolov et al.[1, 23]. The junction under study is incorporated into a superconducting loop. This loop is then inductively coupled to a dc-SQUID magnetometer. Figure 3.1 shows a schematic of the setup. By passing a current through the junction's loop it causes a flux proportional to the phase. The flux can be measured using the inductively coupled dc-SQUID. It also allows us to determine the current through the junction. This means we have all the information we need in order to reconstruct the CPR. This chapter first walks through the analysis method and provides arguments for the used assumptions and relations. Subsequently we provide experimental details about the production process of our samples.

3.1 Analysis method

Our method requires little to no analysis, which highlights one of the key benefits of this method. The measurements are performed by passing a current I_t through the junction's loop. Constrained by flux quantisation and the CPR of the junction it will distribute the current between the loop and the junction:

$$I_t = I_s + I_l \tag{3.1}$$

This can be seen by applying Ohm's law to the circuit in Figure 3.1. By simultaneously measuring V_s it is possible to determine $\Phi_s \propto \Phi_l \propto \gamma$. More details on this can be found in Section 3.1.1 and Section 3.1.4.

$$I_l = \frac{\Phi_s}{M} \qquad \Phi_l = \frac{L_l}{M}\Phi_s \tag{3.2}$$

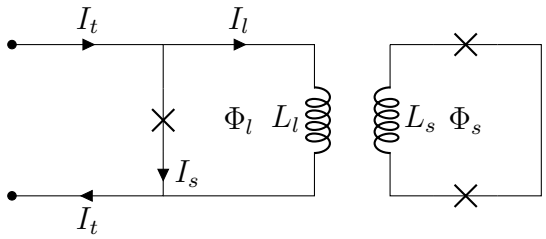

Figure 3.1: *Schematic depiction of the system. The left loop is inductively coupled to the dc-SQUID on the right. This is illustrated by L_l and L_s. The junction under study is part of the left loop and has an inductance L_{JJ}. The current I_t is controlled externally. The flux through the two loops is denoted by Φ_l and Φ_s. Please note that the four contacts used for the dc-SQUID readout are not shown.*

Assuming γ to be proportional to Φ_l we find the phase:

$$\gamma = \frac{2\pi}{\Phi_0}\Phi_l = \frac{2\pi}{\Phi_0}\frac{L_l}{M}\Phi_s \tag{3.3}$$

Arguments for the proportionality between γ and Φ_l are provided in Section 3.1.3. Since we control I_t and indirectly measured I_s we can see that:

$$I_s = I_t - I_l = I_t - \frac{\Phi_s}{M} \tag{3.4}$$

The value for L_l and M can be determined numerically by using the static magnetic response of the superconducting rings. For this purpose the `Python` library `SuperScreen` was used. For more details see [24]. The numerical value might not match the true value, but is also possible to extract L_l from the data by exploiting the fact that the current-phase relation must be 2π periodic, see Section 2.2. Similarly the value for the mutual inductance can be measured indirectly by determining the linear trend we see between Φ_s and I_t. Figure 3.2 shows an example of what the data looks like for a perfectly sinusoidal CPR. The parameters are given in the caption of the figure.

3.1.1 Relation between flux and phase

Using flux quantization and the gauge-invariant phase we can derive a relation between the flux Φ_l and γ. For details please see Appendix A.1.

$$\gamma = \frac{2\pi}{\Phi_0}\left(\Phi_l + \lambda^2\mu_0 \int \vec{J}\cdot d\vec{l}\right) \tag{3.5}$$

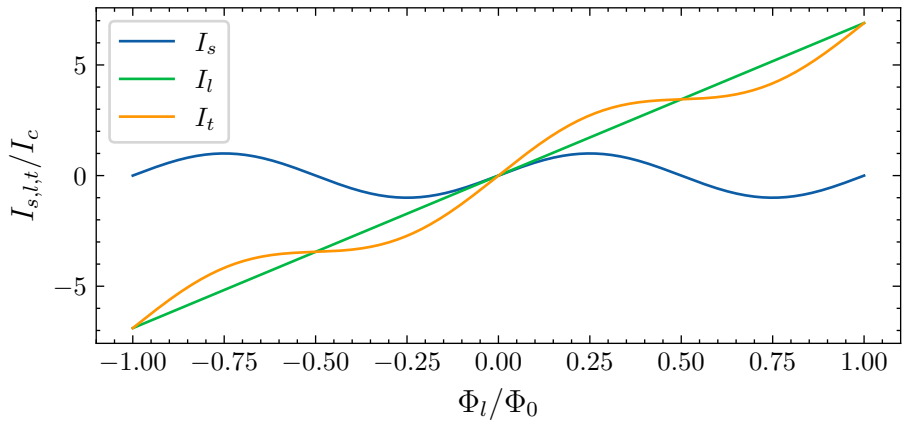

Figure 3.2: *Analytical example showing the super current, loop and total current over loop flux. We used a purely sinusoidal current-phase relation with* $I_c = 300\,\mu\text{A}$ *and a loop inductance of* $1\,\text{pH}$ *such that* $I_c L_l/\Phi_0 \approx 0.05$.

We can express Φ_l in terms of I_s and I_l:

$$\Phi_l = I_s L_{JJ} + I_l L_l \tag{3.6}$$

Where L_{JJ} and L_l are the inductances of the Josephson junction and loop respectively[1]. Strictly speaking L_{JJ} is more of mutual inductance between the loop and the junction. However, in practice it does not matter. We will assume that $L_{JJ} \ll L_l$. This is also done by Frolov et al. (see [1, 23]) and often in literature when discussing dc-SQUIDs (see par example [7]). This means our final equation for the loop flux becomes:

$$\Phi_l = I_l L_l \tag{3.7}$$

3.1.2 Avoiding multi-valued measurements

The linear background can cause multi-valued measurements. To avoid this, the screening parameter[2]:

$$\beta_{\text{rf}} = \frac{2\pi I_c L_l}{\Phi_0} \tag{3.8}$$

should be ≤ 1[1, 7]. This gives a maximum value for the critical current, $I_{c,\max}$ given L_l. Based on an numerical calculation, it appears that for

[1]This is not the so called Josephson inductance but purely a magnetic inductance and not a kinetic inductance.

[2]Normally the screening parameter refers to $\beta_l = 2LI_c/\Phi_0$. However, this is for a 'normal' dc-SQUID and not an rf-SQUID. An rf-SQUID is a superconducting ring with a single Josephson junction.

superconductor-normal-supercoductor (SNS) junctions $\beta_{\text{rf}} < 0.9$ is a more trustworthy criterium. This can be seen in Figure 3.4. This is because the CPR is not perfectly sinusoidal[25, 26]. A prediction for an SNS junction has been plotted in Figure 3.3.

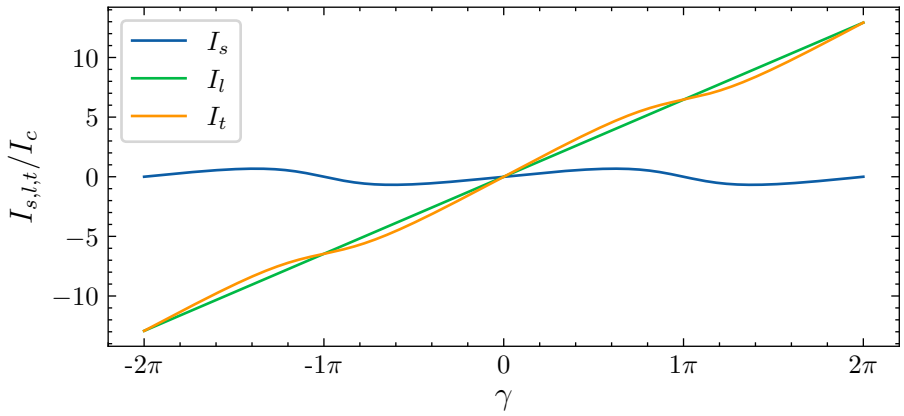

Figure 3.3: *Expectation values for the CPR of an SNS junction. The calculations were done for* $I_c = 100\,\mu\text{A}$, $L_l = 2 \cdot 0.8\,\text{pH}$ *and* $\Delta(T)$ *estimated at* $1\,\text{meV}$. *This means* $\beta_{rf} \approx 0.5$. *We note that the current through the loop creates a linear background that gets modulated by the CPR of the junction. The calculation is done for a short ballistic junction using Equation 2.13 in [25].*

3.1.3 Figure of merit

The goal is to determine γ by measuring Φ_l. The two are only proportional however if the integral term in Equation 3.5 is negligible. As such we have the requirement that:

$$\lambda^2 \mu_0 \int \vec{J} \cdot d\vec{l} \ll \Phi_l$$

We define a figure of merit, δ, that weighs the two terms. The requirement that $\gamma \propto \Phi_l$ is satisfied when $|\delta| \ll 1$.

$$\delta = \frac{\lambda^2 \mu_0 \int \vec{J} \cdot d\vec{l}}{\Phi_l} \tag{3.9}$$

For a square and round geometry the integral part can be rewritten as:

$$\int \vec{J} \cdot d\vec{l} = \begin{cases} 2\pi r \tilde{j} I_l, & \text{round} \\ 8 r \tilde{j} I_l, & \text{square} \end{cases} \tag{3.10}$$

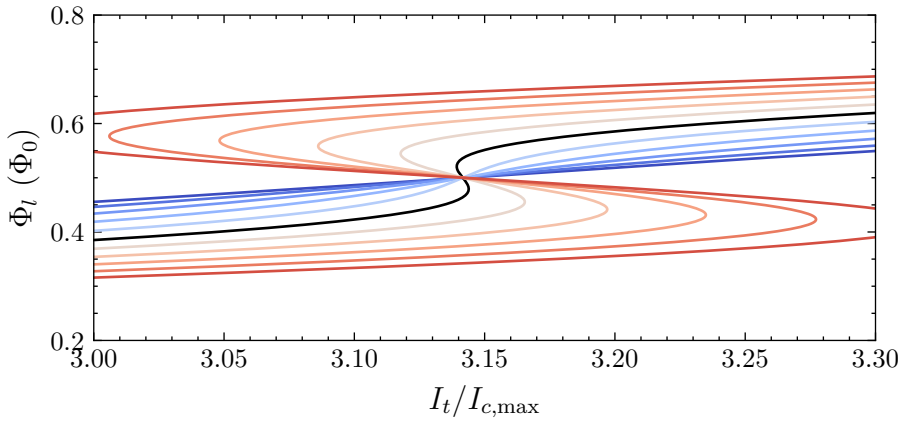

Figure 3.4: *Data produced based on the same parameters as Figure 3.3. This time however we modulated I_c between $0.5I_{c,max}$ (blue) and $1.5I_{c,max}$ (red) in steps of $0.1I_{c,max}$. The black line highlights $I_c = I_{c,max}$. The black line is still slightly multivalued, the reason for this is given in the main text.*

Here r is the radius (half the diameter) and $\tilde{j} = \tilde{j}(d, w, \lambda)$ a geometric factor in m^{-2}. The value of $\tilde{j}$ can be calculated numerically and details can be found in Appendix A.2. The loop flux can be expressed as $\Phi_l = I_l L_l$, this allows us to rewrite the figure of merit as:

$$\delta = \frac{\lambda^2 \mu_0 \tilde{j}}{L_l} \cdot \begin{cases} 2\pi r, & \text{round} \\ 8r, & \text{square} \end{cases} \tag{3.11}$$

It is important to note that the figure of merit only depends on the device geometry and is independent of experimental parameters such as I_l.

3.1.4 Magnetic coupling

The dc-SQUID is inductively coupled to the junction's loop. This means that by measuring Φ_s we can determine Φ_l which is then used to determine γ and I_l. In the experiment a current is passed through the junction's loop. Using the mutual inductance we obtain a relation between I_l and Φ_s:

$$I_l = \frac{\Phi_s}{M} \tag{3.12}$$

Using the inductance of the junction's loop we then also find Φ_l:

$$\Phi_l = I_l L_l = \frac{L_l}{M} \Phi_s \tag{3.13}$$

Our numerical simulation to estimate M does not take into account the possibility of magnetic lensing.[27] As such the mutual inductance might be larger in practice. This means that the dc-SQUID might react more sensitively to changes in the junction's loop.

Having to fit the mutual and loop inductance is one of the weaknesses of our method. In the linear regime of the dc-SQUID extracting the mutual inductance should be trivial. The loop inductance however is determined by the periodicity in the data. Whilst possible to compare the loop inductance to a simulated value, a factor two difference already changes a 2π-periodic CPR to a 4π-periodic current-phase relation. To overcome this, a reference loop without any junction could be added. Alternatively, since the loop inductance also relates to the amplitude of the junction's critical current, it is possible to later cut the junction's loop and measure the critical current of just the junction using a 4-point measurement.

3.2 Sample geometries

The diameter of the dc-SQUID is chosen such that the periodicity of the SQUID interference pattern is on the order of a few mT. This means the effective diameter should be around 1 to 2 µm. Furthermore, the width of the loop together with the thickness of the superconductor determine the geometric factor $\tilde{j}$, they are chosen such that the figure of merit is sufficiently small. In practice this means that the width is around 0.3 µm and the thickness around 100 nm. Details on this can be found on a per sample basis in Chapter 4.

3.3 Sample fabrication

We use a Si substrate of approximately 1 cm^2. The substrate is cleaned by dusting it off using a pressurised nitrogen gas and rinsed for 30 min in acetone in an ultrasonic cleaner. To get rid of acetone residue we rinse it using IPA for 5 min in the ultrasonic cleaner. We spincoat the substrate with a layer of PMMA 600K followed by a layer of PMMA 950K. After this we pattern the sample using electron-beam lithography. Due to the double PMMA layers, development leaves an undercut.

After this process we use dc-sputtering to deposit a 90 nm layer of Nb and cap it using 7 nm of Au. The thickness of the Nb is based on estimations for our figure of merit. The Nb is sputtered in a ultra-high vacuum magnetron

sputtering setup. It has a base pressure of $\leq 1 \cdot 10^{-9}$ mbar and a argon deposition pressure of $4 \cdot 10^{-3}$ mbar. Lift-off is done using acetone. A final rinsing is done using IPA to remove any residues. Using this process we create all the coarse structures. These include the contact pads, leads to the contact pad and a central square in which we will make our fine geometries. Figure 3.5 schematically shows the lithography and sputtering process.

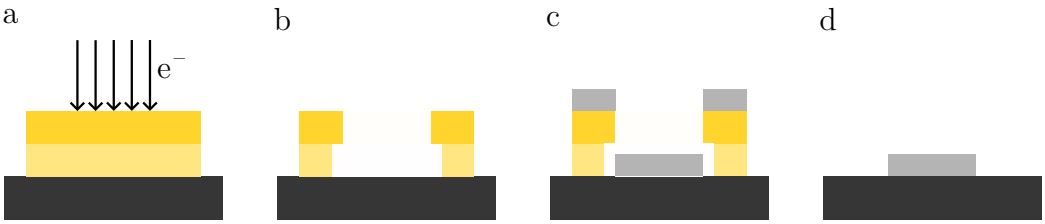

Figure 3.5: *Schematic depiction of the lithography and sputtering process.* ***a)*** *We start with a Si substrate (dark grey) with a layer of PMMA 600K (0.4 µm) and on top of that PMMA 950K (0.4 µm) (yellow) and expose it to an electron beam.* ***b)*** *After exposure, we can remove the exposed regions using MIBK / IPA (1:3).* ***c)*** *We sputter the normal metal and superconductor layers (light grey) on top of the sample.* ***d)*** *In the final step we use acetone for lift-off leaving us with the coarse structures on top of the substrate. The figure is not to scale.*

The finer geometries in the central square are created using focussed ion beam (FIB). They are used to cut away the Nb and Au, leaving just the substrate. The advantage of using the FIB is less PMMA poisoning in our Nb. Figure 3.6 schematically shows the FIB process.

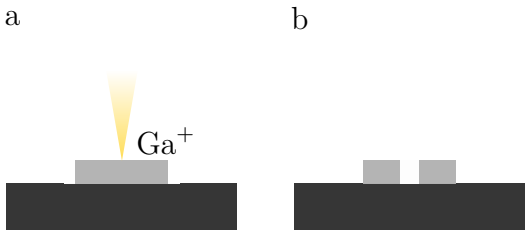

Figure 3.6: *Schematic depiction of the FIB.* ***a)*** *We start with a Si substrate (dark grey) with layer of Nb and Au on top. This was deposited using sputtering. We use a beam of Ga^+ to etch away small pieces of material.* ***b)*** *The regions that have been exposed to the Ga^+ beam are gone. The figure is not to scale.*

Chapter 4

Samples

In this chapter our results are presented on a per sample basis. The results of the first sample, CP1, are not directly useful towards our goal. However, it has thought us a great deal about working with the setup and proved relevant in choosing the geometries for the second sample, CP2. The second sample produced the first real results and shows the feasibility of the method. In our final sample, CP3, further improvements were made based on the results of the second sample. This sample was destroyed before any useful measurements were taken. It has been included because of its potential for future research. After this sample CP2 was revisited and produced the bulk of our important results.

4.1 Sample CP1

4.1.1 Fabrication

This sample uses lateral constriction junctions (ScS)[1] fabricated by FIB milling. The advantage of these junctions is that the behaviour of the depends strongly on ξ. As such, due to the temperature dependence of ξ we can tune the junction behaviour. The size of the constriction should ideally be around 3ξ.[26]

Our method benefits from a small λ, as can be seen in our figure of merit (Section 3.1.3). As such we used Nb as our superconductor[2]. At 0 K Nb has $\lambda = 47\,\text{nm}$ and $\xi = 38\,\text{nm}$.[28]

[1] Also called a Dayem bridge, see [26].

[2] Other candidates were NbTi and MoGe, they however have a much larger penetration

Parameter	Value
junction's loop $\varnothing_{\text{outer}}$ / $\varnothing_{\text{inner}}$	2.1 µm / 1.5 µm
dc-SQUID $\varnothing_{\text{outer}}$ / $\varnothing_{\text{inner}}$	1.6 µm / 1.2 µm
spacing	0.4 µm
d_{Nb}	113 nm
d_{Au}	7 nm

Parameter	Value
L_l	4.9 pH
L_s	4.4 pH
M	−0.1 pH
L_l/M	−88.2
δ	0.397

Table 4.1: *The* ***left*** *table provides an overview of the geometries of CP1.6H as determined by SEM imaging and sputtering rates. The* ***right*** *table gives an overview of parameters found using a simulation based on the geometries. The geometries of the dc-SQUID are based on earlier work by Rog (2022).*

The fabrication followed the method outlined in Section 3.3. Due to a machine malfunction 113 nm of Nb[3] was deposited. The target thickness was 90 nm. The fine structures made using the FIB, can be seen in Figure 4.1. The geometries of the sample can be found in Table 4.1.

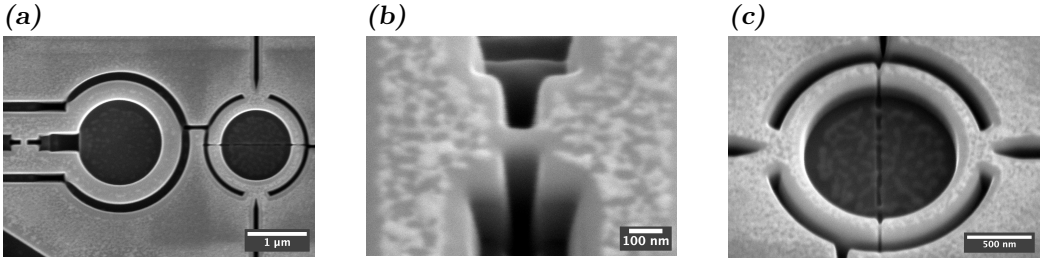

Figure 4.1: *Fine structures of sample CP1 after the FIB. Table 4.1 shows the exact geometries of the sample.* ***a)*** *Overview of the fine structures. On the left we see the junction's loop and on the right the dc-SQUID. The view has been rotated* 90° *clockwise compared to the other figures for visual clarity.* ***b)*** *Zoomed in view of the junction, the size of the junction is* 100 nm *by* 80 nm*. The viewing angle is* 30°*.* ***c)*** *Zoomed in view of the dc-SQUID. The width of the junctions is* 19 nm*. The viewing angle is* 30°*.*

4.1.2 Results and discussion

The measurements were performed in a 1.6 K cryostat equipped with a 7 T magnetic field. While cooling down, a 4-point measurement was used to determine the resistance of the dc-SQUID as a function of temperature. The

depth.

[3]This was measured using an Atomic Force Microscope (AFM) by M. Westerdijk.

RT-curve is shown in Figure 4.2. The sample becomes superconducting at 8 K and has a quite sharp transition. The lower critical temperature compared to pure Nb ($T_c = 9.2\,\mathrm{K}$[28]) is expected when using sputtering methods.

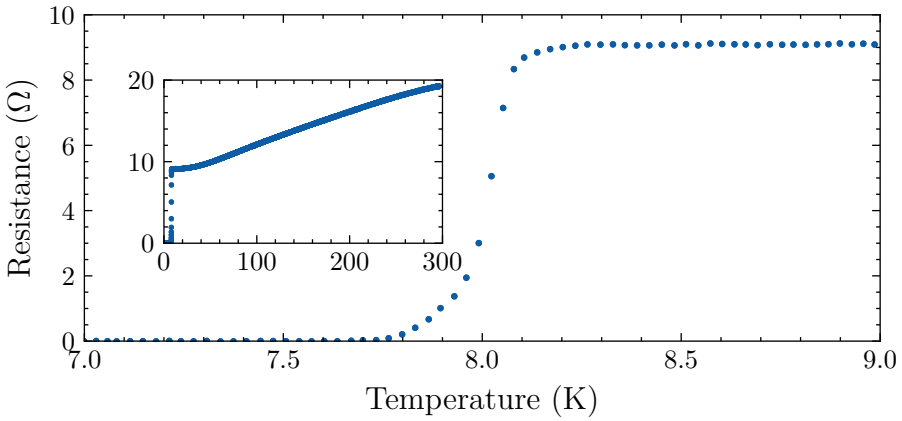

Figure 4.2: *RT-curve of sample CP1. The main figure provides a detailed view of the superconducting transition at* 8 K*. The inset provides an overview of resistance between* 2 *to* 300 K *which is mostly linear.*

Additionally the temperature dependence of the critical current was determined. This is shown in Figure 4.3. There are two transitions starting from 7.2 K, similar to the data in Figure 4.2. The obvious one is a very sharp transition and the second one a more elongated tail. The sharp transition is for the bulk of the superconductor (leads, contact pads, etc.) whilst the more elongated one is from the dc-SQUID's junctions. This defines the range in which the dc-SQUID can be used as a magnetometer. The temperature dependence of the junction behaviour is attributed to the temperature dependence of the coherence length (Section 2.1.1). When the coherence length is relatively small compared to the junction size, then the Cooper pair density can change fast enough to be unbothered by the junction. As such at 7.2 K the junction behaviour disappears.

Figure 4.4 shows the interference pattern of the dc-SQUID at 7.6 K. The periodicity of the interference pattern is between 3 to 3.5 mT. This means the effective area of our dc-SQUID should be between 0.6 to 0.7 µm^2 which corresponds to a diameter between 0.87 to 0.94 µm. However, the SEM images (Figure 4.1) show that the diameter of our effective area must be between 1.2 to 1.6 µm (a periodicity between 1 to 1.8 mT). This larger periodicity suggests that less flux is present in the dc-SQUID.

Flux lensing[27] does not provide an explanation. It would cause a higher flux in the dc-SQUID by focussing the magnetic field and thus a smaller

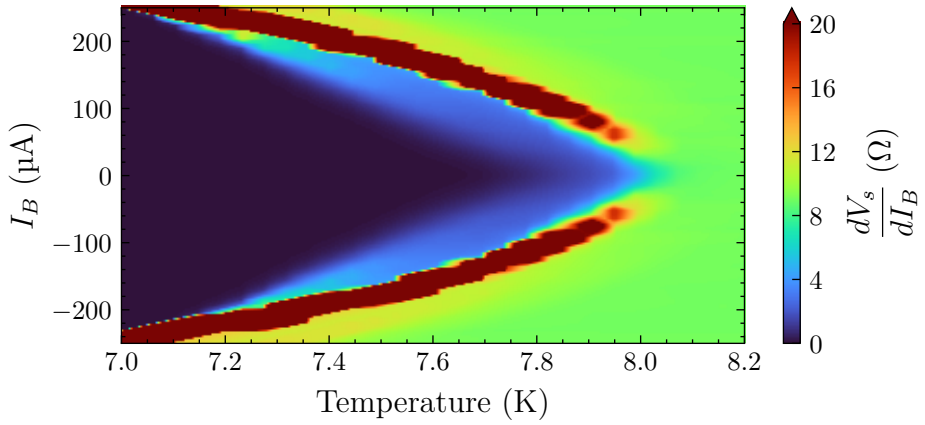

Figure 4.3: *Temperature dependence of the critical current of the dc-SQUID. Near* 7.2 K *an additional region becomes visible before the big transition where the resistance spikes up to above* 20 Ω*.*

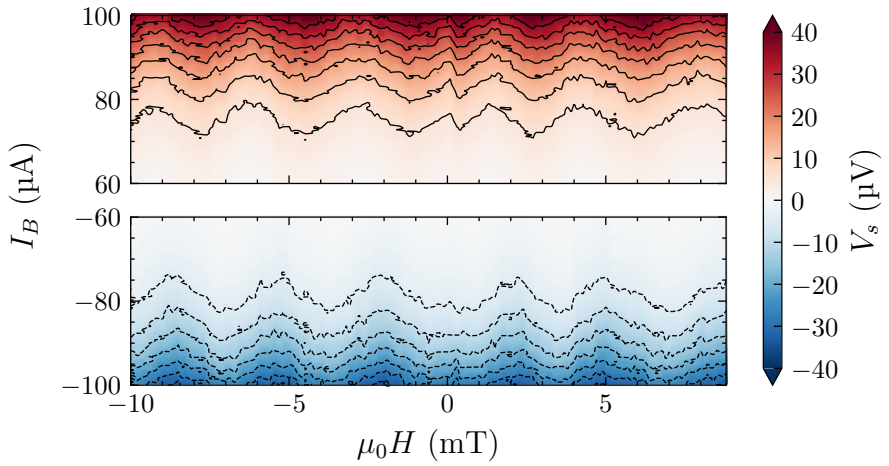

Figure 4.4: *The interference pattern measured over the dc-SQUID at* 7.6 K*. The black lines are equipotential lines spaced* 5 µV *apart.*

periodicity. Furthermore, we trust the scale in the SEM images to be correct. In our view this leaves an field (readout) anomaly as explanation. During our use of the cryostat we later noticed that one of the two power supplies of the magnet was turned off. The current supplies operate in parallel, as such only half the current could be delivered effectively. If the magnet does not independently measure how much current is delivered then this would explain the factor two difference. As such we believe that this caused the incorrect field (readout). This hypothesis is further supported by the fact that the magnet was not able to produce more than 4 T fields. Due to time constraints

however we have not been able to definitively test this hypothesis.

Furthermore, the highest sensitivity of the dc-SQUID (in the linear regime) is 18 to 21 $\mu V \cdot mT^{-1}$ (or 36 to 42 $\mu V \cdot mT^{-1}$ if the field (readout) was indeed off by a factor two). Compared to dc-SQUIDs produced in our group earlier this is not good. Par example [8] reported a dc-SQUID with similar geometries[4] and a sensitivity around 105 $\mu V \cdot mT^{-1}$. Improving the sensitivity of our current device further would be difficult because we are already near the critical current where we go through the bulk transition. Changing the temperature would be an option, however since taking a SQUID interference pattern takes a long time it was not viable due to the limited measurement time. Measurements at a constant bias current were attempted but did not work due to software limitations.

Finally, an attempt was made to measure the CPR at 7.6 K[5]. To do so we biased the dc-SQUID at 200 µA and sweeped a current through the junction's loop from −250 to 250 µA and simultaneously measured the voltage over the dc-SQUID. The measured IV-curve looked very similar to the IV-curve of the dc-SQUID at 7.6 K. This does not make sense and the measurement probably failed for the following two reasons. Firstly, the bias current through the dc-SQUID was too high, pushing it into its normal regime. This can be seen in Figure 4.3. Secondly, there most likely was a short between some of the connections. The first issue could have been fixed easily, but was only noted too late. The second issue was not investigated further due to time constraints. Even if we had done so we likely would not have been able to fix it in a timely manner. More people in our group reported issues with this specific batch of Si wafers. As such it appears to be a likely culprit.

[4]The junctions were however SNS junctions and not constriction junctions as a layer of Ag was present.

[5]Due to the poor dc-SQUID performance we did not expect this to be extremely fruitful. However it is a quick measurement and would not hurt.

4.2 Sample CP2

This sample's goal was to fix the shortcomings of our first sample. The first thing we want to improve is the dc-SQUID sensitivity and its useable temperature range. To do so SNS junctions were used instead of constriction junctions. SNS junctions were used in our group before and yielded good results.[8] Furthermore, in order to mitigate any chance of shorts we use a Si with a thermal oxide on top. Additionally, to improve the coupling between the dc-SQUID and the junction's loop we used a square geometry instead of a circular one.

4.2.1 Fabrication

In addition to the method outlined in Section 3.3, a layer of Cu was sputtered first. This enables the creation of superconductor-normal-superconductor (SNS) junctions. Additionally a Si wafer with a 300 nm thermal oxide layer was used. Figure 4.5 shows the fine structures created using the the FIB. Contrary to the first sample, a square geometry was used instead of a circular one. This improves the coupling between the junction's loop and the dc-SQUID.

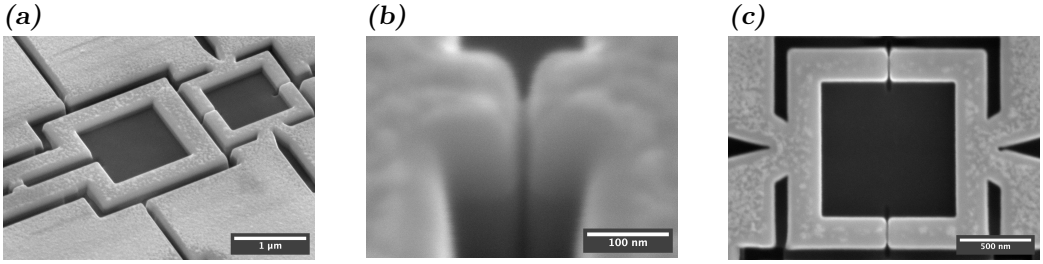

Figure 4.5: *Fine structures of sample CP2 after the FIB. Table 4.2 shows the exact geometries of the sample.* ***a)*** *Overview of the device. The top loop shows the dc-SQUID and the bottom is the junction's loop. The viewing angle is* 30° *and the view has been rotated slightly.* ***b)*** *Zoomed in view of the junction, the width of the junction is* 12 nm *and* 16 nm *across. The viewing angle is* 30°*.* ***c)*** *Zoomed in view of the dc-SQUID. The width of the junctions is* 22 nm*.*

4.2.2 Results and discussion

Figure 4.6 shows the RT-curves for the junction's loop and dc-SQUID. The critical temperature for the bulk of the sample is lower (7 K) compared to the first sample (8 K). This can be explained by the proximity effect due to

Parameter	Value
junction's loop $\varnothing_{\text{outer}}$ / $\varnothing_{\text{inner}}$	1.9 µm / 1.2 µm
dc-SQUID $\varnothing_{\text{outer}}$ / $\varnothing_{\text{inner}}$	1.6 µm / 1.1 µm
spacing	0.1 µm
d_{Cu}	25 nm
d_{Nb}	70 nm
d_{Au}	7 nm

Parameter	Value
L_l	3.1 pH
L_s	3.2 pH
M	−0.2 pH
L_l/M	−17.5
δ	0.012

Table 4.2: *The* ***left*** *table provides an overview of the geometries of CP2 as determined by SEM imaging and sputtering rates. The* ***right*** *table gives an overview of parameters found using a simulation based on the geometries. The geometries are based on sample CP1.*

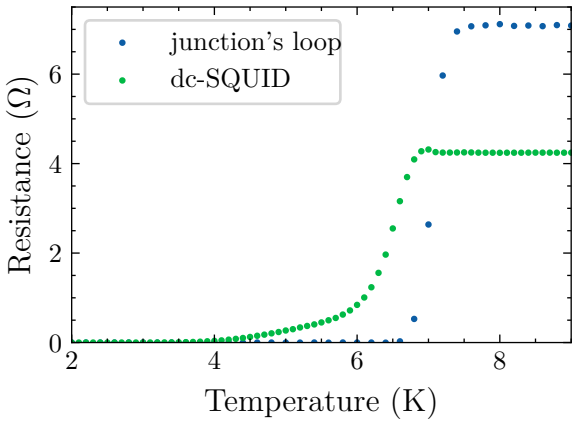

Figure 4.6: *Temperature dependences of the 4-point resistance measured over the dc-SQUID and the junction's loop. We note that just before the superconducting transition that there is a small bump in resistance of the dc-SQUID and a long 'tail' before reaching 0 Ω. The transition of the junction's loop is much sharper in comparison.*

the interface between the Cu and Nb.[29] The longer 'tail' is characteristic for SNS junctions due to the proximity effect.

Figure 4.7 shows the interference pattern of the dc-SQUID for several bias currents. The periodicity in the the data is roughly 1 mT. This matches the expected period. Furthermore, the sensitivity in the linear regime increased by a factor 10 compared to the previous sample. The comparison is a bit unfair as the bias current was 3 times as large. In the previous sample however, such a large bias current was simply not possible. There are two issues with this result. First off, the period of the pattern does not seem to be constant. Secondly, the offset (in the field axis) varies a lot between curves whilst they should all be zero. Both these issues can be explained by vortices getting trapped in the magnet or sample.

During an attempt to measure the CPR, the IV-curves showed anomalous

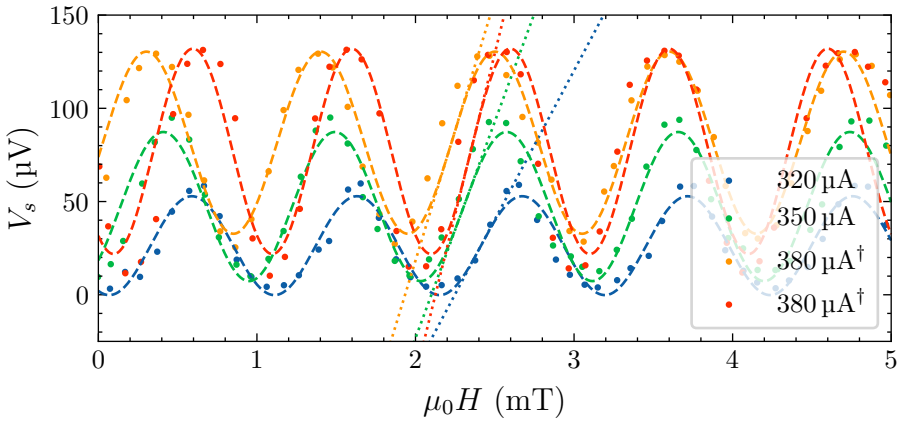

Figure 4.7: *Voltage measured over the dc-SQUID for various bias currents over external magnetic field. The patterns have been fitted to a sinusoid and the slanted lines illustrate the linear response. The sensitivities in the linear regions are* 160, 232, 279 *and* 346 µV/mT *respectively. For* 380 µA *the curve has been measured twice (annotated with a †).*

spikes. Initially we attributed this to vortex trapping. However, upon closer inspection these jumps are exactly correlated with the actual magnetic field reported by the magnet controller. Figure 4.8 shows a clear overlap between the dc-SQUID voltage and the magnetic field as measured by the magnet. Even though a constant setpoint of 0 mT was used, there is quite some drift. This is because the magnet does not have a persistent mode but instead uses a feedback loop to keep a constant field. This feedback loop has a dead band of 50 µT. Changing the setpoint of the field or the rate of change did not have a significant effect.

In an attempt to fix the 'noise' caused by the feedback loop, the magnet was turned off. Unfortunately, it never turned back on as the magnet controller was broken. A downside of this, is that it was no longer possible to read out the value of the field. An attempt was made to measure the CPR again by using a constant bias current of 380 µA for the dc-SQUID. It should be mentioned that during these measurements there appeared to be a lot of drift causing measurements to differ widely. An external magnetic field was likely responsible for this. Possibly this was still caused by the magnet controller as, later on when it was replaced, this did not seem to be an issue anymore.

Figure 4.9 shows the raw data from one of the CPR measurements. There is a clear periodicity in the signal of around 200 µA and a somewhat linear trend on top of that. This specific measurement is presented because it has no unexpected jumps in the dc-SQUID voltage; has a sufficiently small sample

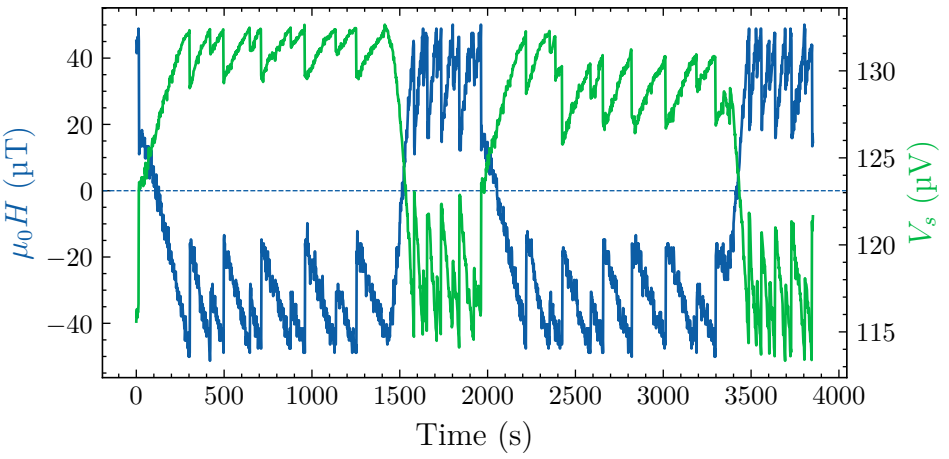

Figure 4.8: *Correlation between the actual magnetic field of the cryostat and the voltage measured over the dc-SQUID. The setpoint of the magnetic field is* 0 mT *and a change rate of* $200\,\mu\mathrm{T}\cdot\mathrm{s}^{-1}$. *The standard deviation from the setpoint is* 30 µT.

spacing; covers a wide enough range to see several periods; and measured both positive and negative currents. Using different sample spacings did not affect the measured periodicity.

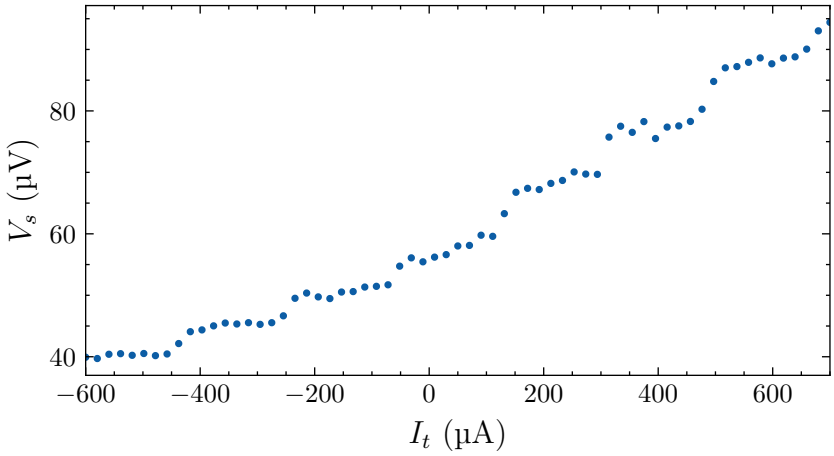

Figure 4.9: *The voltage over the dc-SQUID over the applied total current. A bias current through the dc-SQUID of* 380 µA *was used, the measurement was done at* 3 K.

Using the second calibration curve for 380 µA bias current we converted the dc-SQUID voltage to a flux. A linear fit is used to determine the mutual inductance to be -0.339 ± 0.005 pH. This is almost twice as large as the

simulated value in Table 4.2. Similarly, by exploiting the Φ_0-periodicity of the CPR, the junction's loop's inductance was found to be $6 \pm 1\,\mathrm{pH}$. Again this is almost twice the as large as the simulated value in Table 4.2. Using the proportionality between Φ_l and γ the flux was converted to a phase. Figure 4.10 shows the result of this analysis.

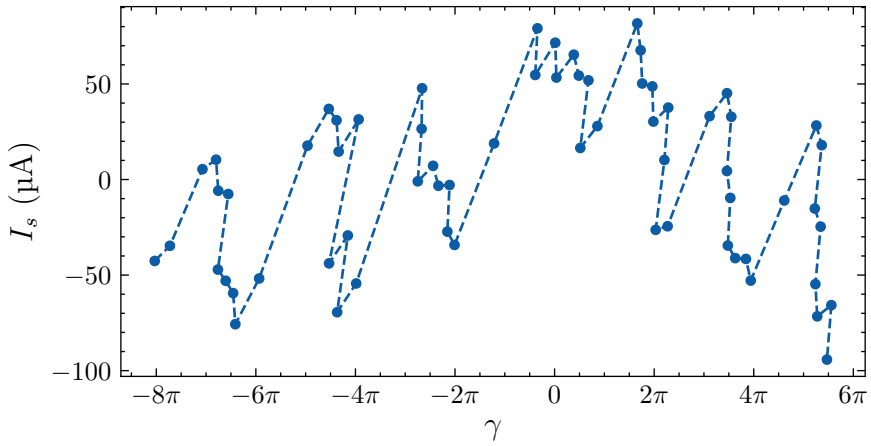

Figure 4.10: *Supper current through the junction's loop over junction's loop flux. See main text for details on how this result was obtained. The dashed line is to improve visual clarity.*

The amplitude of the oscillations is around 60 µA and the pattern contains quite steep slopes. Furthermore, the pattern 'dips' down a bit and does not oscillate around the same mean. Most likely this is because the dc-SQUID is not biased in its linear regime and thus a measurement artefact.

It is clear that two major issues with this result are the lack of resolution and the calibration. Future measurements should take much smaller steps. Furthermore, because it was not possible to keep the dc-SQUID in the linear response region the sensitivity and calibration were suboptimal.

4.3 Sample CP3

4.3.1 Fabrication

We suspect that the sharp edges in the CPR from sample CP2 might be caused by multi-valued measurements. $\beta_{rf} \approx 0.91$ for the previous sample according to our result. In order to get a $\beta_{\mathrm{rf}} < 0.9$ we decided to lower the inductance. Alternatively we could have lowered the critical current. To do so we could have created the junction's loop with a smaller inner diameter.

Additionally, in order to more accurately control the flux through the dc-SQUID we add a modulation line. This allows us to bias the dc-SQUID in the linear regime without the need for an external field. Furthermore it also enables the use for a flux-locked loop (FLL). The implementation of the modulation line is based on [30].

As an alternative we considered making a third loop identical to the junction's loop without a junction. We could then pass a current through it in order to bias the dc-SQUID and use a FLL. The advantage of this method would be that we can directly determine the mutual inductance between this loop and the dc-SQUID. This would by extension give us the mutual inductance between the dc-SQUID and junction's loop. However, this method was deemed impossible because a current of $10\,\mathrm{mA} \gg I_c$ would be required in order to bias the dc-SQUID to a half Φ_0.

The FLL is implemented digitally using proportional and integral (PI) feedback. A deviation $\delta V_s = V_s - V_{s,\mathrm{setpoint}}$ is measured and the modulation current adjusted accordingly. The deviation is caused by the current through the junction's loop as well as noise. By measuring a specific I_t for a longer period we can accurately determine the (average) modulation current required to compensate δV_s. Because the deviation caused by noise should average out, we are left with the contribution of just the junction's loop coupling. This averaged value can be used to determine Φ_l more accurately.

Digital feedback can be tuned more easily than analogue feedback. Due to time constraints this is an important factor at present. Future project should consider using analogue feedback as it can be done more accurately. As a reference see Section 4.2.2 in *SQUID Readout Electronics and Magnetometric Systems for Practical Applications*[31].

We used a triangular geometry for our dc-SQUID to improve the coupling to the junction's loop.

(a) ***(b)***

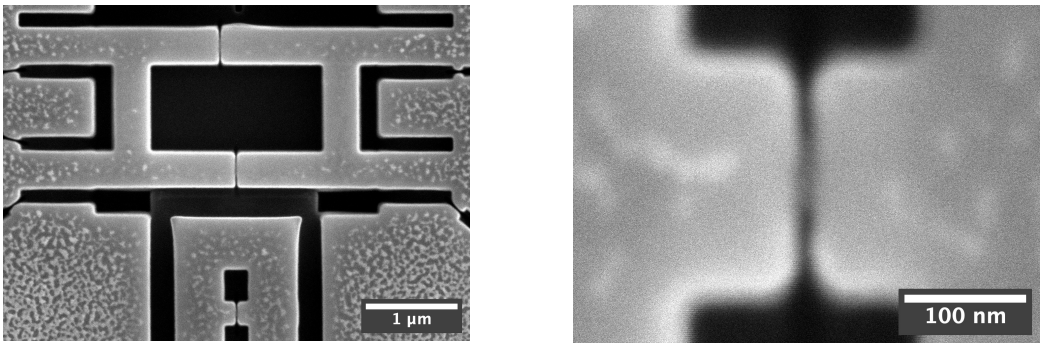

Figure 4.11: *Fine structures of sample CP3 after the FIB. Table 4.3 shows the exact geometries of the sample.* ***a)*** *Overview of the device. The top loop shows the dc-SQUID and the bottom is the junction's loop.* ***b)*** *Zoomed in view of the junction, the width of the junction is* 12 nm.

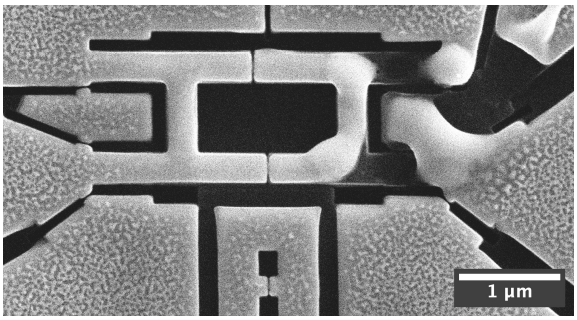

Figure 4.12: *The remains of sample CP3. Figure 4.11 shows what the sample originally looked like. Most of the damage occurred in the superconducting lead for the dc-SQUID readout.*

4.3.2 Results and discussion

The sample sadly enough exploded and we were unable to produce any (significant) results. Its remains are shown in Figure 4.12. The location of the damage is unexpected. It would be more logical if the junctions had exploded as those are the most fragile due to higher current densities.

There is one noteworthy result for this sample. During our measurements it appeared as though the sample has two critical temperatures. The RT-curves are shown in Figure 4.13. The bulk transition of the dc-SQUID appears to be around 7.5 K. The junction's loop transitions around 6 K. In hindsight we think the cause is a significant delay between the sample's thermometer and the sample itself. The delay has not been noted before as we took resistance measurements every few seconds instead of waiting for temperature stability. This could easily be checked if it the sample was still alive.

Regardless of these setbacks we do still think that the ideas behind the sample

Parameter	Value
junction's loop $\varnothing_{\text{outer}}$ / $\varnothing_{\text{inner}}$	1.0 µm / 0.3 µm
dc-SQUID $\varnothing_{\text{outer}}$ / $\varnothing_{\text{inner}}$	2.0 µm / 1.4 µm
	1.3 µm / 0.7 µm
spacing	0.1 µm
d_{Cu}	25 nm
d_{Nb}	70 nm
d_{Au}	10 nm

Parameter	Value
L_l	0.8 pH
L_s	2.8 pH
M	−0.1 pH
L_l/M	−15.3
δ	0.023

Table 4.3: *The* ***left*** *table provides an overview of the geometries of CP3 as determined by SEM imaging and sputtering rates. The* ***right*** *table gives an overview of parameters found using a simulation based on the geometries. For the dc-SQUID two diameters are shown as it is slightly rectangular.*

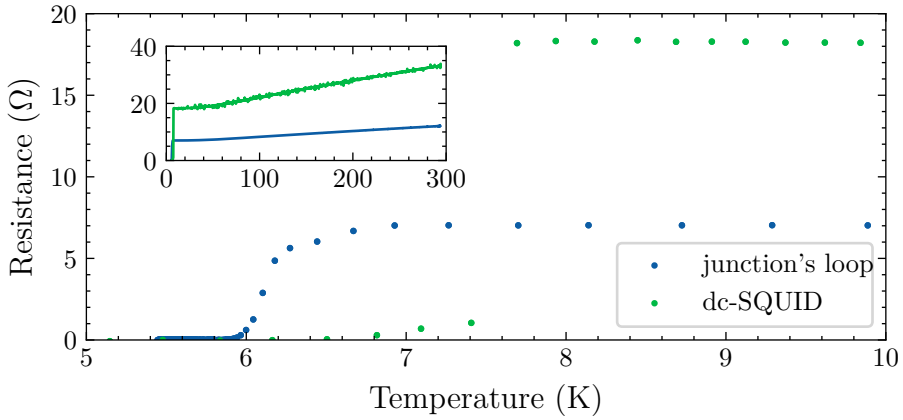

Figure 4.13: *Temperature dependences of the 4-point resistance measured over the dc-SQUID and the junction's loop. The inset shows the RT-curves from* 0 *to* 300 K. *The main figure highlights the superconducting transitions. The junction's loop resistance is quite sharp. The dc-SQUID transition again has a 'tail'. A reason for the difference in critical temperature is given in the main text.*

are promising. We suspect that the damage is caused by using two current sources in parallel. Future experiments might want to use a summing amplifier combined with a VI-converter or a Howland circuit.

4.4 Sample CP2 revisited

After the failure of sample CP3 we revisited sample CP2. By increasing the temperature it is possible to lower I_c. This opens the possibility to go into a non-multivalued regime by decreasing the screening parameter. Refer to Section 3.1.1 for more information. The reason this was not attempted earlier is because the magnet controller was broken. As such it was not possible to measure SQIs at higher temperatures and consequently to measure the CPR at higher temperatures. The sample has not been altered, so the reader is referred to Section 4.2.1 for the geometries.

4.4.1 Results and discussion

The sample had not been permanently stored in a desiccator. Worst case it had been exposed for a few days. An important check was thus if the sample had degraded. The RT-curve of the dc-SQUID showed no significant changes. As such it is unlikely that the sample degraded significantly. It also confirmed that all the contacts are still good.

Previously the CPR was measured at 3 K. An increase in temperature decreases the sensitivity of our dc-SQUID and the critical current of the junction's loop. Our previous measurement has a periodicity of 200 µA. In order to see multiple periods it is preferable to change I_t between ±400 µA. This allows us to see around 4 to 5 periods. Through trial and error we found the highest usable temperature to be 3.6 K.

Similarly to last time, SQIs were measured for several bias currents ranging from 300 to 350 µA. The SQIs shown in Figure 4.14. Whilst the SQIs are far from perfect, they are usable. Near zero field the periodicity as well as the horizontal offset is reproducible. The amplitude of the oscillations is stable as well. Since the junction's loop will only create a small flux this should be sufficient. Around zero field we can approximate the oscillations as sinusoidal. After fitting it gives a sensitivity of 491.37, 189.73, 326.49, 410.49 and 419.73 $\mu V \cdot {\Phi_0}^{-1}$ for 2.8, 3.0, 3.2, 3.4 and 3.6 K respectively. These are comparable to previous results. Please note that the first sensitivity is significantly higher due to a higher bias current.

After the calibrations the current-phase relations were measured. They are shown in Figure 4.15. From the slope in our data we determined the mutual inductance to be 0.4 times the simulated value in Table 4.2. For the loop inductance the value is 3.5 times the simulated value. These deviations might be explained by the fact that the simulation does not take the layer of Cu into

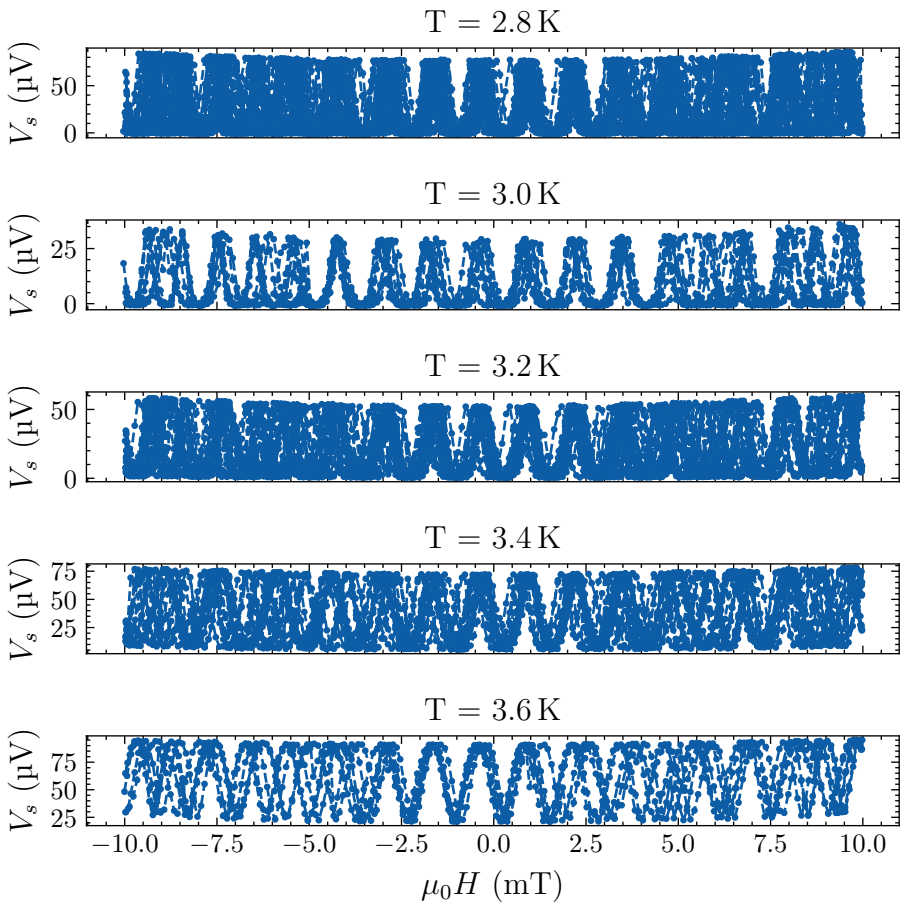

Figure 4.14: *SQIs at 2.8 to 3.6 K of sample CP2. We note that they appear to have a slightly curved background. We used a bias current of 300 µA except for 2.8 K where 350 µA was used. Near zero field the patterns seem quite stable but further out become more noisy.*

account. Additionally these values do not match what we previously found for this sample. Possibly this is because the calibration was not optimal. The amplitude of the oscillations decreases when the temperature increases except for the measurement at 3.6 K. We suspect that this deviation at 3.6 K is due to a human error. A likely explanation is that a different bias current was used for the dc-SQUID compared to the bias current used for the calibration.

Ignoring the measurement at 3.6 K, the critical current goes from 90 to 45 µA between 2.8 to 3.4 K. Figure 4.16 shows the CPR at different temperatures for both a short diffusive and short ballistic SNS junction. Qualitatively we see that our results best match the short ballistic CPR. In either case we see

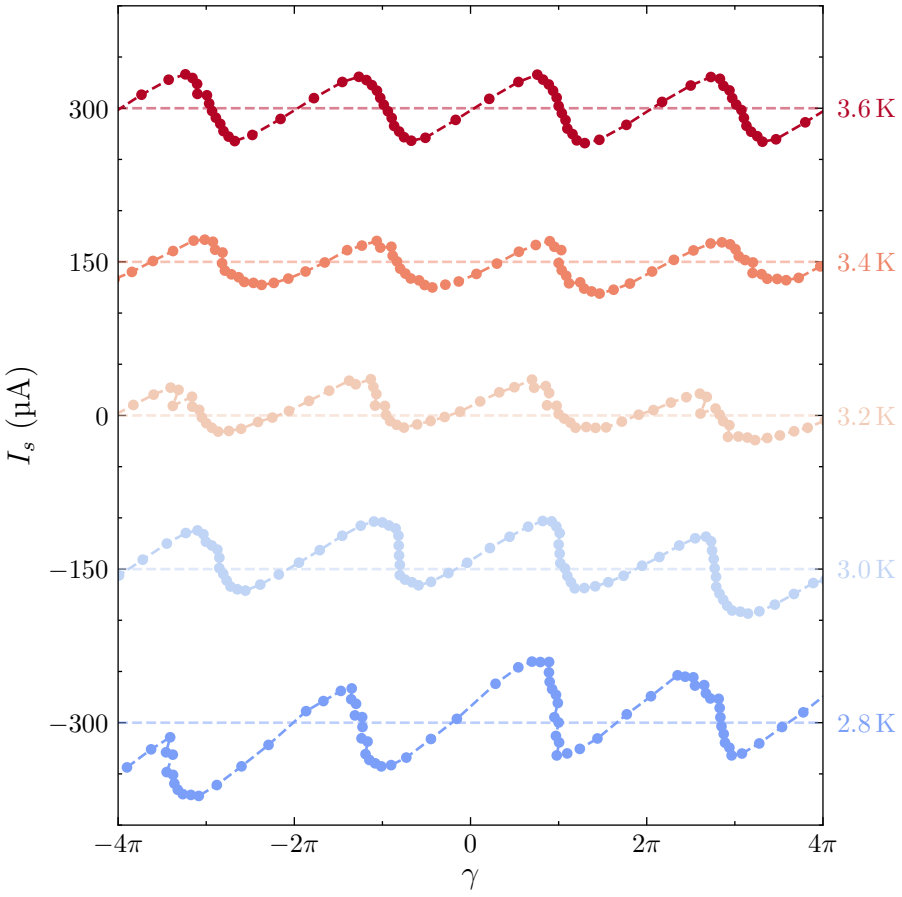

Figure 4.15: *Various current-phase relations measured on sample CP2 in a range of* 2.8 *to* 3.6 K. *The CPRs have been visually offset by* 150 µA. *The horizontal dashed lines denote zero current. The lines through the data points are for visual clarity.*

that the CPR becomes more sinusoidal and that the amplitudes decrease as the temperature increases.

It is odd that that the short ballistic model qualitatively matches the data better. Especially since a gaussian pattern was observed when doing higher field measurements on the dc-SQUID. A gaussian pattern is expected with diffusive behaviour.[8, 32] Another possibility is that our junction is diffusive but that we are in a multi-valued regime.

Clearly the results show a few artefacts most notably at 2.8, 3.0 and 3.4 K. We attribute this to the fact that we are not in the linear regime of our dc-SQUID. We are confident that if the dc-SQUID would be biased in the

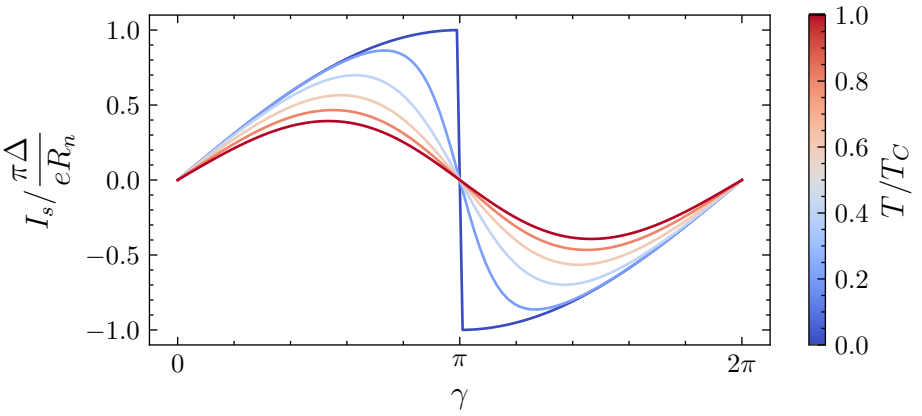

(a) *Theoretical CPRs at different temperatures for a short ballistic SNS junction, see Equation 2.13 in [25].*

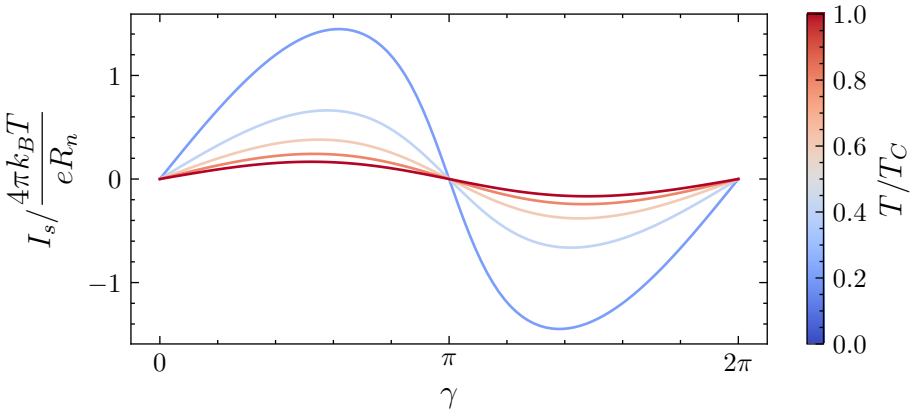

(b) *Theoretical CPRs at different temperatures for a short diffusive SNS junction, see Equation 2.14 in [25].*

Figure 4.16: *Theoretical predictions for the CPR of both a short ballistic and short diffusive SNS junction. In both cases Δ has been estimated at* 1 meV.

linear regime that these artefacts would disappear. Additionally because we did not control our dc-SQUID's bias, it is not possible to say what point $\gamma = 0$. As such we have artificially centred the curves such that $\gamma = 0$ for $I_s = 0$.

Chapter 5

Conclusion

In this thesis a method to measure the current-phase relation of a Josephson junction was developed and its performance demonstrated. Our method utilises a dc-SQUID inductively coupled to a superconducting loop with a single junction. By passing a current through the junction's loop it is possible to modulate the phase of the junction. This phase is proportional to the flux in the loop which is measured by the dc-SQUID. From the total current and the measured flux the current-phase relation can be extracted.

The temperature dependence of the current-phase relation of a SNS junction was qualitatively determined using the above method. Starting from 2.8 to 3.6 K the 2π-periodic current-phase relation becomes more sinusoidal as the critical temperature is approached. Furthermore between 2.8 to 3.4 K we determined the critical current to decrease from 90 to 45 µA. Both these observations are in line with theoretical models. However, the data does not yet allow us to distinguish between diffusive and ballistic behaviour.

Whilst successful, further improvements are possible. Most notably the implementation of a flux-locked loop. This will allow biasing the dc-SQUID at its working point. This means that the measurements will become more sensitive. Furthermore, a flux-locked loop allows integrating the results over a longer period improving the accuracy. An attempt was made to implement the flux-locked loop using a current modulation line. However, that sample was unfortunately destroyed. Future projects can use its design.

5.1 Outlook

The potential of the method has been demonstrated. Future research should improve the method. The most promising improvement is the addition of a flux-locked loop dc-SQUID readout scheme that improves the sensitivity and decreases unwanted background interference. In order to measure the current-phase relation of Sr_2RuO_4 minor adjustments to the method are needed. It is impractical to make both the junction's loop and the dc-SQUID from the same crystal. But we can use our electron-beam-induced deposition facilities to directly deposit superconducting WC next to the junction under study. Furthermore, we currently lack the knowledge on how to pin a single chiral domain wall. As such it is difficult to study a single chiral domain wall. Alternatively, it might be possible to incorporate a ring of Sr_2RuO_4 with two chiral domain walls instead of a single junction. In that case no additional weak links must be formed, or their behaviour negligible compared to the Sr_2RuO_4 ring.

Appendix A

Derivations

A.1 Phase-flux relation

The magnetic field $\vec{B}$ can be written as the curl of the magnetic vector potential $\vec{A}$. This allows the magnetic flux through the superconducting loop to be rewritten in terms $\vec{A}$.

$$\Phi = \oiint \vec{B} \cdot d\vec{a} = \oiint \left(\nabla \times \vec{A}\right) \cdot d\vec{a} = \oint \vec{A} \cdot d\vec{l} \tag{A.1}$$

The closed integral over $\vec{A}$ can be any path enclosing the hole in the superconductor. It consists of two pieces, namely the junction and the rest of the loop.

$$\Phi = \int_{\mathrm{JJ}} \vec{A} \cdot d\vec{l} + \int_{\mathrm{loop}} \vec{A} \cdot d\vec{l} \tag{A.2}$$

For the integral over the junction we use the gauge-invariant phase (Equation 2.5).

$$\gamma = \Delta\varphi_{\mathrm{JJ}} - \frac{2\pi}{\Phi_0} \int_{\mathrm{JJ}} \vec{A} \cdot d\vec{l} \Rightarrow \int_{\mathrm{JJ}} \vec{A} \cdot d\vec{l} = \frac{\Phi_0}{2\pi} \left(\Delta\varphi_{\mathrm{JJ}} - \gamma\right) \tag{A.3}$$

For the integral over the rest of the loop we use the superfluid velocity[1]:

$$m^* \vec{v} = 2m_e \vec{v} = \hbar \nabla \varphi - \frac{e^* \vec{A}}{c} \overset{\mathrm{SI}}{=} \hbar \nabla \varphi + 2e\vec{A} \tag{A.4}$$

[1] See *Introduction to Superconductivity* equation 4.9, the equation has been converted to SI units.

Rewriting the equation gives:

$$\vec{A} = \frac{1}{2e}\left(\hbar\nabla\varphi_{\text{loop}} - 2m_e\vec{v}\right) \tag{A.5}$$

Substituting $\vec{v}$ with a more useable expression in terms of the current density $\vec{J}$ and λ using Equation 2.3.

$$\vec{J} = -2e|\Psi|^2\vec{v} = -\frac{m_e}{\lambda^2 e\mu_0}\vec{v} \Rightarrow \vec{v} = -\frac{\lambda^2 e\mu_0}{m_e}\vec{J} \tag{A.6}$$

Combining the two equations gives us a useable expression for $\vec{A}$ in the loop:

$$\begin{aligned}\vec{A} &= \frac{1}{2e}\left(\hbar\nabla\varphi_{\text{loop}} + 2\lambda^2 e\mu_0\vec{J}\right) \\ &= \frac{\Phi_0}{2\pi}\nabla\varphi_{\text{loop}} + \lambda^2\mu_0\vec{J}\end{aligned} \tag{A.7}$$

Going back to Equation A.2:

$$\begin{aligned}\Phi &= \underbrace{\frac{\Phi_0}{2\pi}\left(\gamma - \Delta\varphi_{\text{JJ}}\right)}_{\int_{\text{JJ}}\vec{A}\cdot d\vec{l}} \underbrace{-\frac{\Phi_0}{2\pi}\Delta\varphi_{\text{loop}} - \lambda^2\mu_0\int\vec{J}\cdot d\vec{l}}_{\int_{\text{loop}}\vec{A}\cdot d\vec{l}} \\ &= \frac{\Phi_0}{2\pi}\left(\gamma - \underbrace{\left(\Delta\varphi_{\text{JJ}} + \Delta\varphi_{\text{loop}}\right)}_{\text{Multiple of } 2\pi}\right) - \lambda^2\mu_0\int\vec{J}\cdot d\vec{l}\end{aligned} \tag{A.8}$$

The phase must wind by a multiple of 2π to make sure that the wave function is uniquely defined at each point. Using this fact and the quantization of Φ in units of Φ_0 we get:

$$\Phi = \left(\frac{\Phi_0}{2\pi}\gamma - \lambda^2\mu_0\int\vec{J}\cdot d\vec{l}\right) \mod \Phi_0 \tag{A.9}$$

$$\gamma = \frac{2\pi}{\Phi_0}\left(\Phi + \lambda^2\mu_0\int\vec{J}\cdot d\vec{l}\right) \tag{A.10}$$

A.2 Geometric factor $\tilde{j}$

The goal of this appendix section is to derive how to calculate $\tilde{j}$. In a rectangular thin film superconductor with thickness (height) d on the order of λ

and width $w > \lambda$ such that $wd \gg \lambda$ then the current density a distance x from the centre is given by[33]:

$$J(x) = \begin{cases} \frac{J(0)}{\sqrt{1-\left(\frac{2x}{w}\right)^2}} & 0 \leq x \leq \frac{\lambda^2}{2d} \\ \frac{J(w/2)}{\exp\left(d\frac{w/2-x}{\lambda^2}\right)} & \frac{\lambda^2}{2d} < x \leq w/2 \end{cases} \tag{A.11}$$

The value for $J(w/2)$ can be found by stitching the two solutions together at $x = \frac{\lambda^2}{2d}$. To find $\tilde{j}$ we take the integral from 0 to $w/2$ over $J(x)$. Multiplying by the height d gives the current through the thin film. This is proportional to $J(0)$ and invites us to define $J(0) = \tilde{j}I$ where I is the total current.

$$\begin{aligned} I = J(0)/\tilde{j} &= 2d \int_0^{w/2} J(x)dx \\ \tilde{j} &= \frac{J(0)}{2d \int_0^{w/2} J(x)dx} \end{aligned} \tag{A.12}$$

Since the integral is proportional to $J(0)$ the end result for $\tilde{j}$ only depends on the geometries of the sample and not the current I. This also means that the result for $\tilde{j}$ is valid for all currents. This integral quite possibly has an analytical solution, however we used SciPy to perform the integration numerically.

Bibliography

[1] S. M. Frolov, D. J. Van Harlingen, V. A. Oboznov, V. V. Bolginov, and V. V. Ryazanov, *Measurement of the Current-Phase Relation of SFS pi-Josephson junctions*, (Feb. 17, 2004) `http://arxiv.org/abs/cond-mat/0402434` (visited on 01/09/2023), preprint.

[2] M. Tinkham, *Introduction to Superconductivity*, 2nd ed. (Dover Publications), 454 pp.

[3] A. P. M. Place, L. V. H. Rodgers, P. Mundada, B. M. Smitham, M. Fitzpatrick, Z. Leng, A. Premkumar, J. Bryon, A. Vrajitoarea, S. Sussman, G. Cheng, T. Madhavan, H. K. Babla, X. H. Le, Y. Gang, B. Jäck, A. Gyenis, N. Yao, R. J. Cava, N. P. de Leon, and A. A. Houck, "New material platform for superconducting transmon qubits with coherence times exceeding 0.3 milliseconds", Nat Commun **12**, 1779 (2021).

[4] I. V. Pechenezhskiy, R. A. Mencia, L. B. Nguyen, Y.-H. Lin, and V. E. Manucharyan, "The superconducting quasicharge qubit", Nature **585**, 368–371 (2020).

[5] F. Zhang, M. T. Ahari, A. S. Rashid, G. J. de Coster, T. Taniguchi, K. Watanabe, M. J. Gilbert, N. Samarth, and M. Kayyalha, *Reconfigurable magnetic-field-free superconducting diode effect in multi-terminal Josephson junctions*, arXiv.org, (Jan. 12, 2023) `https://arxiv.org/abs/2301.05081v1` (visited on 06/13/2023).

[6] C. Ciaccia, R. Haller, A. C. C. Drachmann, C. Schrade, T. Lindemann, M. J. Manfra, and C. Schönenberger, *Gate Tunable Josephson Diode in Proximitized InAs Supercurrent Interferometers*, arXiv.org, (Apr. 2, 2023) `https://arxiv.org/abs/2304.00484v2` (visited on 06/13/2023).

[7] J. Clarke and I. Braginski, *The SQUID Handbook*, Vol. 1, 2 vols. (Wiley, 2004).

[8] M. Rog, "SQUID-on-tip Magnetic Microscopy using Tunneling-Based Height Control", (2022).

[9] J. R. Prance and M. D. Thompson, "Sensitivity of a DC SQUID with a non-sinusoidal current-phase relation in its junctions", Applied Physics Letters **122**, 222601 (2023).

[10] A. Murani, A. Kasumov, S. Sengupta, Y. A. Kasumov, V. T. Volkov, I. I. Khodos, F. Brisset, R. Delagrange, A. Chepelianskii, R. Deblock, H. Bouchiat, and S. Guéron, "Ballistic edge states in Bismuth nanowires revealed by SQUID interferometry", Nat Commun **8**, 15941 (2017).

[11] M. Endres, A. Kononov, H. S. Arachchige, J. Yan, D. Mandrus, K. Watanabe, T. Taniguchi, and C. Schönenberger, "Current–Phase Relation of a WTe $_2$ Josephson Junction", Nano Lett. **23**, 4654–4659 (2023).

[12] M. Kayyalha, A. Kazakov, I. Miotkowski, S. Khlebnikov, L. P. Rokhinson, and Y. P. Chen, "Highly skewed current–phase relation in superconductor–topological insulator–superconductor Josephson junctions", npj Quantum Mater. **5**, 1–7 (2020).

[13] E. Strambini, A. Iorio, O. Durante, R. Citro, C. Sanz-Fernández, C. Guarcello, I. V. Tokatly, A. Braggio, M. Rocci, N. Ligato, V. Zannier, L. Sorba, F. S. Bergeret, and F. Giazotto, "A Josephson phase battery", Nat. Nanotechnol. **15**, 656–660 (2020).

[14] D. B. Szombati, S. Nadj-Perge, D. Car, S. R. Plissard, E. P. a. M. Bakkers, and L. P. Kouwenhoven, "Josephson 0-junction in nanowire quantum dots", Nature Phys **12**, 568–572 (2016).

[15] K. Lahabi, "Spin-triplet supercurrents of odd and even parity in nanostructured devices" (Leiden University, Dec. 4, 2018).

[16] M. Sigrist and D. F. Agterberg, "The Role of Domain Walls on the Vortex Creep Dynamics in Unconventional Superconductors", Progress of Theoretical Physics **102**, 965–981 (1999).

[17] J. Yao, "Spin Transport and Superconductivity in Half-metallic Nanowires and Junctions" (Leiden University, Leiden, 2023), 128 pp.

[18] M. L. Della Rocca, M. Chauvin, B. Huard, H. Pothier, D. Esteve, and C. Urbina, "Measurement of the Current-Phase Relation of Superconducting Atomic Contacts", Phys. Rev. Lett. **99**, 127005 (2007).

[19] F. E. Schmidt, M. D. Jenkins, K. Watanabe, T. Taniguchi, and G. A. Steele, *Probing the current-phase relation of graphene Josephson junctions using microwave measurements*, (July 19, 2020) `http://arxiv.org/abs/2007.09795` (visited on 01/13/2023), preprint.

[20] J. Bardeen, L. N. Cooper, and J. R. Schrieffer, "Theory of Superconductivity", Phys. Rev. **108**, 1175–1204 (1957).

[21] A. A. Golubov, M. Y. Kupriyanov, and E. Il'ichev, "The current-phase relation in Josephson junctions", Rev. Mod. Phys. **76**, 411–469 (2004).

[22] M. Schmelz and R. Stolz, "Superconducting Quantum Interference Device (SQUID) Magnetometers", in *High Sensitivity Magnetometers*, Vol. 19, edited by A. Grosz, M. J. Haji-Sheikh, and S. C. Mukhopadhyay (Springer International Publishing, Cham, 2017), pp. 279–311.

[23] S. M. Frolov, "Current-phase relations of Josephson junctions with ferromagnetic barriers" (University of Illinois at Urbana-Champaign, 2005), 149 pp.

[24] L. Bishop-Van Horn and K. A. Moler, "SuperScreen: An open-source package for simulating the magnetic response of two-dimensional superconducting devices", Computer Physics Communications **280**, 108464 (2022).

[25] J. Vermeer, "STM-based Scanning SQUID Microscopy: A novel magnetic imaging technique" (Leiden University, Leiden, 2-07-21).

[26] K. K. Likharev, "Superconducting weak links", Rev. Mod. Phys. **51**, 101–159 (1979).

[27] L. Prigozhin and V. Sokolovsky, "3D simulation of superconducting magnetic shields and lenses using the fast Fourier transform", Journal of Applied Physics **123**, 233901 (2018).

[28] B. W. Maxfield and W. L. McLean, "Superconducting Penetration Depth of Niobium", Phys. Rev. **139**, A1515–A1522 (1965).

[29] C. Cirillo, S. L. Prischepa, M. Salvato, C. Attanasio, M. Hesselberth, and J. Aarts, "Superconducting proximity effect and interface transparency in Nb/PdNi bilayers", Phys. Rev. B **72**, 144511 (2005).

[30] J. Lin, B. Müller, J. Linek, M. Karrer, M. Wenzel, M. J. Martínez-Pérez, R. Kleiner, and D. Koelle, "YBa $_2$ Cu $_3$ O $_7$ nano superconducting quantum interference devices on MgO bicrystal substrates", Nanoscale **12**, 5658–5668 (2020).

[31] Y. Zhang, H. Dong, H.-J. Krause, G. Zhang, and X. Xie, *SQUID Readout Electronics and Magnetometric Systems for Practical Applications*, 1st ed. (Wiley, July 20, 2020).

[32] F. Chiodi, M. Ferrier, S. Guéron, J. C. Cuevas, G. Montambaux, F. Fortuna, A. Kasumov, and H. Bouchiat, "Geometry-related magnetic interference patterns in long S N S Josephson junctions", Phys. Rev. B **86**, 064510 (2012).

[33] E. Rhoderick and E. Wilson, "Current Distribution in Thin Superconducting Films", Nature **194**, 1167–1167 (1962).